Torque Control of an In-Wheel Axial Flux Permanent Magnet Synchronous Motor using a Fuzzy Logic Controller for Electric Vehicles

Vo Thanh Ha
Faculty of Electrical and Electronics Engineering, University of Transport and Communications, Vietnam
vothanhha.ktd@utc.edu.vn
(corresponding author)

Received: 17 January 2023 | Revised: 31 January 2023 | Accepted: 3 February 2023

ABSTRACT

This paper presents the control design of an in-wheel axial-flux permanent magnet synchronous motor with one stator and one rotor, using a fuzzy logic controller for electric vehicles. In this controller, the surgeon ambiguous inference file is built by two input vectors, the stator current error and the derivative of the stator error. These input variables include five membership functions: Negative Big (NB), Negative Small (NS), Equal Zero (ZE), Positive Small (PS), and Positive Big (PB). The fuzzy logic controller was implemented using a 5×5 matrix to meet the required output stator voltage of the controller. The fuzzy logic torque controller was compared with the PI controller in stator current response, torque, and speed. The proposed controller was evaluated using simulation results from MATLAB/SIMULINK.

Keywords-AFPMSM; fuzzy logic; PI; FOC; Electrical Vehicles (EVs)

I. INTRODUCTION

Electric cars are a revolutionary trend in today transportation. Electric cars have advantages compared to cars with internal combustion engines as they eliminate complicated gearboxes and emissions and are environmentally friendly [1-2]. The powertrain structure of Electric Vehicles (EVs) tends to use an in-wheel distributed electric drive system consisting of multiple motors, which ensures traction at the front or rear of a car on two or four wheels, using a front, rear, or four-wheel drive system [3-4]. This electric powertrain improves driving performance by differentiating between wheels, makes full use of vehicle energy, improves transmission efficiency, increases range, eases braking, has good heat dissipation, and is more convenient for installation and maintenance [5-6]. The Axial Flux Permanent Magnet Synchronous Motor (AFPMSM) is widely used in in-wheel motor drive systems because it has short shaft length characteristics, is lightweight, has good vibration resistance, and has a long service life, thus improving reliability and safety [7]. Although AFPMSM motors enhance the performance of EVs, each vehicle should have installed multiple motors, resulting in a complex control system [8]. In-wheel motors increase the cost of a vehicle and have high requirements for control procedures, such as power balancing, electronic differential, and energy recovery. In addition, electric car in-wheel motors require small size, light weight, small torque, high efficiency, large overload capacity, and wide speed range [9]. Therefore, scientists have been interested in studying the control of traction and torque of in-wheel AFPMSMs and their response to wheels. Torque and speed controllers are controlled based on Direct Torque Control (DTC) and Field-Oriented Control (FOC). These controllers are designed using linear and nonlinear control methods such as PI, LQR, dead beat, sliding mode, flatness, fuzzy [10-14], or hybrid controllers such as fuzzy-neural, fuzzy-sliding, and PI-fuzzy [14-17]. However, the torque response has a slight pulsation, and the actual speed response quickly and accurately tracks the required speed [17-20]. Therefore, the study of intelligent control solutions to improve an integrated in-wheel AFPMSM torque in an EV should be combined with the required components and physical properties, such as brake and accelerator pedals, road inclination, and wind resistance. Consequently, these parameters are necessary to improve the performance and torque of EVs.

This study presents the control design of an in-wheel AFPMSM, one stator, and one rotor, using a Fuzzy Logic Controller (FLC) for EV systems. In this controller, the surgeon ambiguous inference file is built by two input vectors, the stator current error and the derivative of the stator error. These input variables include five membership functions, Negative Big (NB), Negative Small (NS), Equal Zero (ZE), Positive Small (PS), and Positive Big (PB). The FLC was implemented with a 5×5 matrix so that the output stator voltage of the controller is met. The fuzzy logic torque controller was compared with the PI controller in stator current response, torque, and speed.

II. MODEL AND CONTROL OF THE ELECTRIC CAR POWER SYSTEM

A. Mathematical Model of an AFPMSM

It is possible to utilize the standard PMSM model for an AFPMSM. Stator parameters, such as the inductor calculation, change between the two models. Furthermore, the Back-EMF produced by an excitation coil and a permanent magnet is the same. Therefore, the radial PMSM of a AFPMSM and the model are mathematically related. The stator voltage equation in the *d-q* frame of reference is given by:

$$V_q = R_q + \frac{d}{dt}\lambda_q + \omega_e \lambda_d \quad (1)$$

$$V_d = R_d I_d + \frac{d}{dt}\lambda_d - \omega_e \lambda_q \quad (2)$$

The stator voltage equation is as follows:

$$\underline{u}_s^s = R_s . \underline{\iota}_s^s + \frac{d\underline{\psi}_s^s}{dt} \quad (3)$$

where R_s is the stator resistance and $\underline{\psi}_s^s$ is the stator flux. Then, converting (3) from the phase winding system of the stator to the coordinate system, quasi-rotor flux gives:

$$\underline{u}_s^f = R_s . \underline{\iota}_s^f + \frac{d\underline{\psi}_s^f}{dt} + j\omega_s \underline{\psi}_s^f \quad (4)$$

The relationship between stator and rotor flux is described by:

$$\underline{\psi}_s^f = L_s \underline{\iota}_s^f + \underline{\psi}_p^f \quad (5)$$

where $\underline{\psi}_p^f$ is the polar flux vector. Since the *d*-axis of the coordinate system coincides with the axis of the polar flux, the perpendicular component (*q*-axis) of $\underline{\psi}_p^f$ will be zero. Thus, the flux vector has only real components.

$$\left|\underline{\psi}_p^f\right| = \psi_p \quad (6)$$

The equation of flux components is given by:

$$\begin{cases} \psi_{sd} = L_{sd} i_{sd} + \psi_p \\ \psi_{sq} = L_{sq} i_{sq} \end{cases} \quad (7)$$

where i_{sd}, i_{sq} are the *d* and *q* coordinate stator currents, and L_{sd}, L_{sq} are the *d* and *q* coordinate inductance. Substituting (5) and (6) into (4) and passing through the *d-q* coordinate system gives the system of equations of the PMSM motor:

$$\begin{cases} u_{sd} = L_{sd}\frac{di_{sd}}{dt} + R_s i_{sd} - \omega_e L_{sq} i_{sq} \\ u_{sq} = L_{sq}\frac{di_{sq}}{dt} + R_s i_{sq} + \omega_e L_{sd} i_{sd} + \omega_e \psi_f \end{cases} \quad (8)$$

The torque of the motor is described by:

$$T_m = \frac{3}{2} P_p \left[\psi_f i_{sq} + \left(L_{sd} - L_{sq}\right) i_{sd} i_{sq}\right] \quad (9)$$

The motor torque is comprised of two components: the primary component $\psi_f i_{sq}$ and the reactive component. To create a control system, the stator current vector must be adjusted so that the vertical current vector is parallel to the polar flux. Therefore, there is a torque-generating current component, not a magnetizing current component, and motor torque is given by:

$$T_m = \frac{3}{2} P_p \psi_f i_{sq} \quad (10)$$

B. Mathematical Model of the Electric Vehicle

The gearbox model shows the angular speed and torque relationships according to the gear ratio $k_{gear} \prec 1$, as shown in:

$$\begin{cases} T_m k_{gear} = T_{Wh} \\ \omega_{Wh} = \omega_m k_{gear} \end{cases} \quad (11)$$

where T_m is the motor torque, T_{Wh} is the torque acting on the wheel, $T_i = T_{Wh}$ is the load torque, and *J* is the inertia torque of the motor. Applying Newton's second law in the rotation of the motor gives:

$$T_{em} - T_{Wh} = J\frac{d\omega_m}{dt} \quad (12)$$

The drive wheel model can be expressed as:

$$\begin{cases} v_{Wh} = \omega_{Wh} R_{Wh} \\ T_{Wh} = T_L = F_t R_{Wh} \end{cases} \quad (13)$$

The vehicle will act on the road surface with a force *F* while the wheel is resting on it with a force *N* and is being propelled by a torque T_{wh}. In contrast, the road surface will act against the vehicle with a point of the same value in the opposite direction of F_t. In this scenario, the reasonable force that propels the car at speed is the frictional force F_t given by:

$$F_t = m_v . g . \mu \quad (14)$$

where μ is the grip coefficient. The following equation results from applying Newton's second law to the parts of the outside force operating on the vehicle's body:

$$m_v \frac{dv_{ev}}{dt} = F_t - F_{aero} - F_{roll} - m_v . g . sin(\alpha) \quad (15)$$

Air resistance is given by:

$$F_{aero} = \frac{\rho C_d A_F}{2}(v_{ev} + v_{wind})^2 \quad (16)$$

In some cases, the wind speed can be set to $V_{wind} = 0$. The rolling resistance exists in the case of an underinflated tire and can be given by:

$$F_{roll} = f_r F_{zY} \quad (17)$$

$$F_{zY} = m_v g\, cos(\alpha) \quad (18)$$

where F_{zY} is the vertical surface reaction and f_r is the rolling resistance coefficient.

III. FLC TORQUE CONTROLLER DESIGN

The FLC controls the system by calculating the necessary voltages u_{sd} and u_{sq} so that the difference between the currents i_{sd} and i_{sq} is as tiny as possible. The exactly planned i_{sd} and i_{sq} stator currents are used to regulate the motor's torque control current. This paper outlines the modern controller design for the i_{sd} and the control strategy for an in-wheel AFPMSM, one stator, and one rotor, utilizing an FLC. This controller uses the stator current error and the derivative of the stator error as the two input vectors to build the ambiguous inference file.

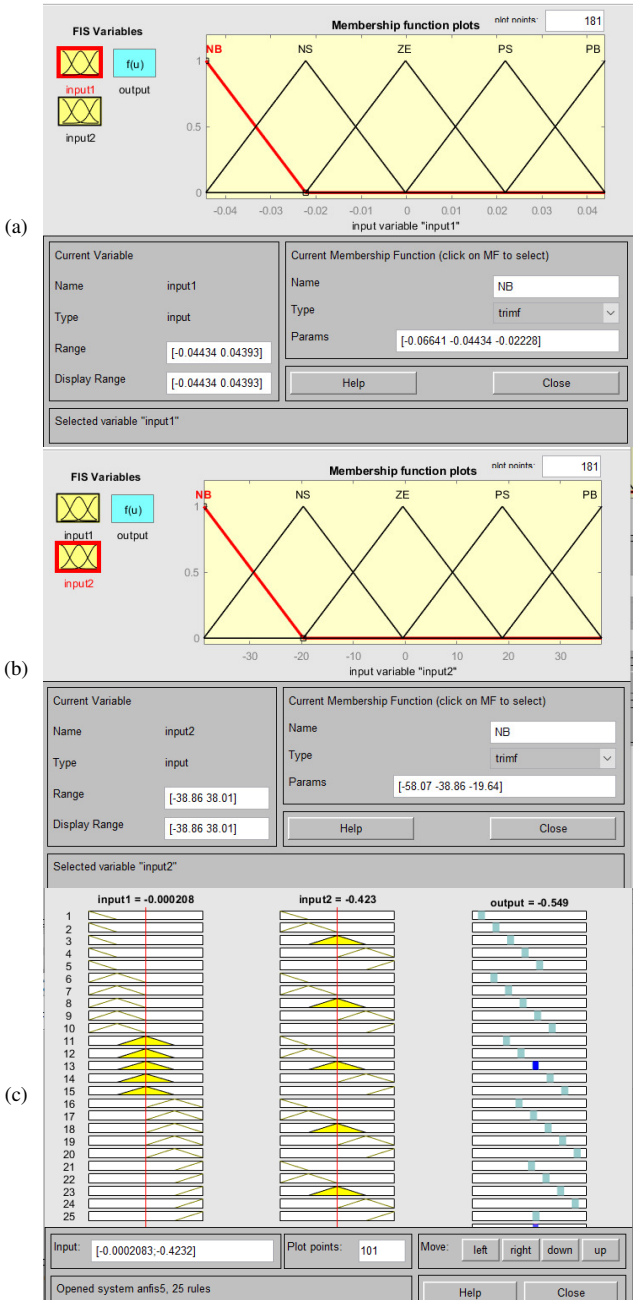

Fig. 1. (a), (b) Inputs, (c) output, and fuzzy rules of the FLC controller.

The input variables include five membership functions: Positive Big (PB), Positive Small (PS), Equal Zero (ZE), Negative Big (NB), and Negative Small (NS). Table I and Figure 1 show the FLC constructed using a 5×5 matrix. The FLC consists of 25 rules, which are implemented as follows:

- If (input 1 is NB) and (input 2 is NB), then (output is NB)
- If (input 1 is NB) and (input 2 is NS), then (output is NB)
- If (input 1 is NB) and (input 2 is ZE), then (output is NB)
- If (input 1 is PB) and (input 2 is PB), then (output is PB)

TABLE I. MATRIX OF FLC CONTROLLER

Input 1 (e) / Input 2 (Δe)	**NB**	**NS**	**ZE**	**PS**	**PB**
NB	NB	NB	NB	NS	ZE
NS	NB	NB	NS	ZE	PS
ZE	NS	NS	ZE	PS	PB
PS	ZE	ZE	PS	PB	PB
PB	ZE	PS	PB	PB	PB

IV. SIMULATION RESULTS

A. Building Trajectories of Accelerator, Brake, and Operating Modes of Electric Vehicles

The trajectories of accelerators and brakes of electric cars are built according to a function *F*(*x1, x2, …xn*). Figure 2 shows the trajectories of the accelerator and brakes. The *F* function can be obtained experimentally and the output is calculated by looking up or interpolating the defined table using the block parameters according to a method, such as linear (linear gradient), Lagrange (Linear Lagrange), closest point, block spline, and Akima spline interpolation. The Fcos function can range in size from 1 to 30. The first and second inputs define the row and column dimension breakpoints, respectively. Figure 3 shows the determination of the accelerator and brake trajectories.

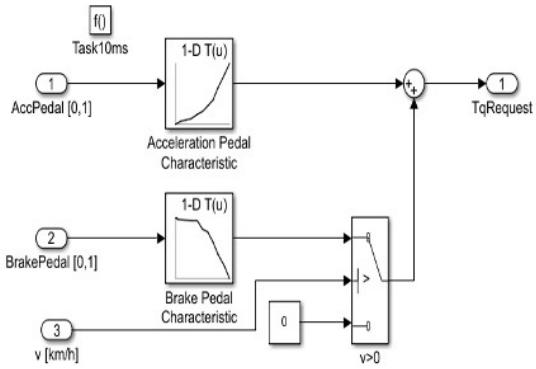

Fig. 2. The trajectories of the accelerator and brakes.

Breakpoints	Column	(1)
Row		--
(1)	**0**	0
(2)	**0.1**	8.2
(3)	**0.2**	14.35000...
(4)	**0.30000...**	20.5
(5)	**0.4**	32.8
(6)	**0.5**	41
(7)	**0.6**	61.5
(8)	**0.7**	82
(9)	**0.8**	123
(10)	**0.9**	164
(11)	**1**	205

Breakpoints	Column	(1)
Row		--
(1)	**0**	0
(2)	**0.03**	0
(3)	**0.04**	-8.2
(4)	**0.3**	-10.25
(5)	**0.4**	-12.2999...
(6)	**0.5**	-41
(7)	**0.6**	-51.25
(8)	**0.7**	-82
(9)	**0.8**	-123
(10)	**0.9**	-164
(11)	**1**	-205

Fig. 3. The parameters trajectories of accelerator and brakes.

B. Simulation Results and Evaluation

Figure 4 shows the control structure of the traction drive system for electric cars using the in-wheel AFPMSM, and Table II displays the simulation parameters.

The proposed controller was simulated in MATLAB to evaluate its effectiveness for the traction transmission system in electric cars using an in-wheel AFPMSM, with the following simulation scenario:

- Assume the speed of the wind is 0.
- The car moves on a flat road, but at t = 3.5s to 4.3s, the car goes downhill.
- At time t = 0s, the car starts to accelerate and the accelerator value increases from 0 to 1 after 0.45s. Torque reaches a maximum of 205Nm and remains there for 2s.
- At t = 2s, the vehicle starts to decelerate, and the brake reaches a value from 0 to 1 at t = 3.5s. The torque gradually decreases to -205Nm and returns to 0 at t = 4.66s.

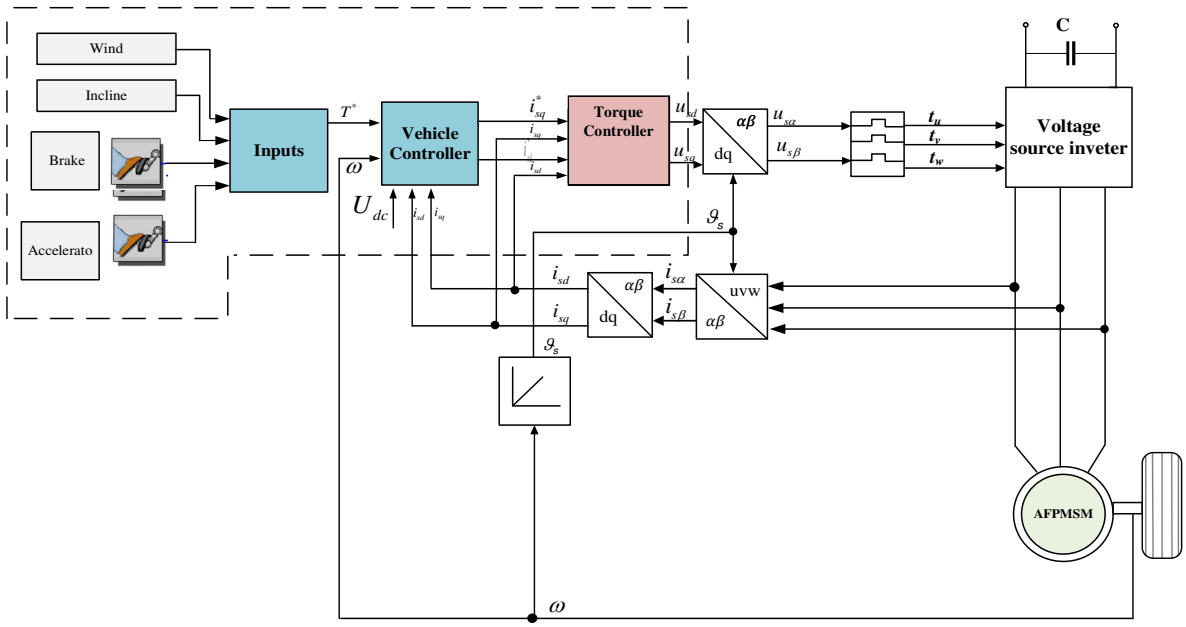

Fig. 4. The control structure for electric cars using an in-wheel AFPMSM motor, based on a FOC method.

TABLE II. PARAMETERS FOR AFPMSM

Motor parameters	Value Symbol	Value
Power	P_{dm}	35Kw
Rated speed	N_{dm}	1800rpm
Rated voltage	U_{dm}	275V
Number of pole pairs	Z_p	8
Magnetic flux density	Ψ	0.0437
Maximum torque	P_{max}	205Nm
Armature resistance	Rs	0.0101Ω
Shaft inductance d	L_d	2.4368e-4H
Shaft inductance q	L_q	2.9758e-4H

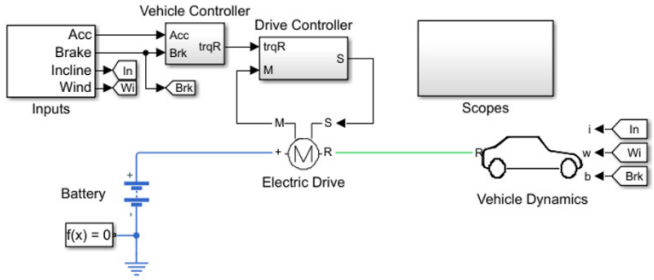

Fig. 5. The MATLAB/SIMULINK control structure for electric cars using an in-wheel AFPMSM.

Table III shows the parameters of the simulated PI controller. Figures 6 and 7 show the stator current responses of the FLC and the PI controller. These figures show that the stator current response in the steady-state method is fast (0.4s) and accurate in the steady-state mode (the actual signal follows the set call). However, the proposed FLC gives better results than the PI controller in over-regulating (no over-throttling), while the PI controller with an over-regulating current at an over-regulating time is 10%. Table IV presents the evaluation criteria for the stator current responses of the PI and the FLC controllers.

TABLE III. PARAMETERS FOR THE PI CONTROLLER

Controller	K_i	K_p
Current controller I_d	7.103004e+2	0.8779
Current controller I_q	1.0615e+3	1.0744

TABLE IV. RESULTS OF EVALUATION RESPONSIBILITY

Controller	PI	FLC
Stator current i_{sd}		
Accelerated setting time (s)	0.4	0.4
Over-adjustment	10%	0%
Stator current i_{sq}		
Set-up time (s)	0.4	0.4
Over-adjustment	10%	0%

(a)

(b)

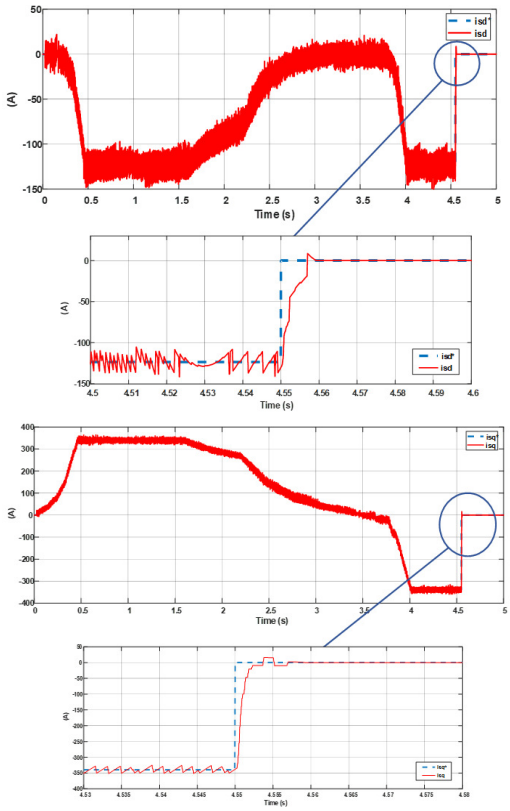

Fig. 6. Stator current responses (a) i_{sd} and (b) i_{sq} for the PI controller.

(a)

(b)

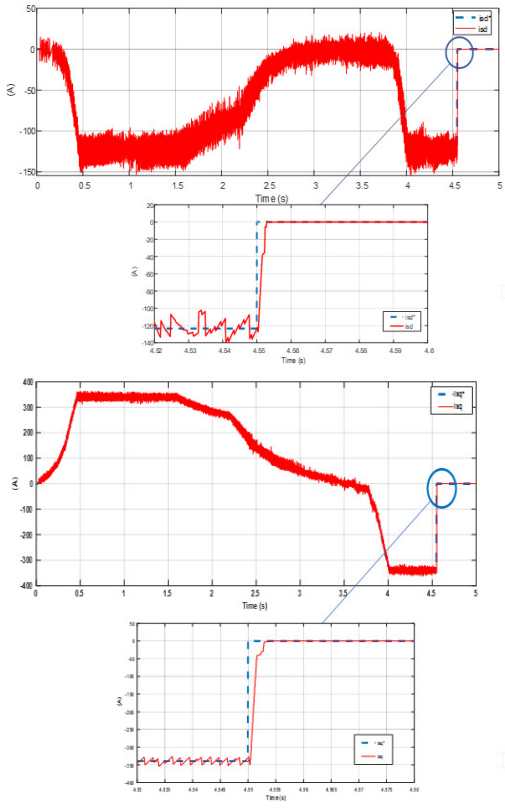

Fig. 7. Stator current responses (a) i_{sd} and (b) i_{sq} for the FLC controller.

Figures 8 and 9 show the comparison of the torque and speed responses of the FLC and the PI controller. These figures show that the torque of the two controllers has the same form as the i_{sq} current. The FLC has less pulse rate (3%) for the torque response than the PI controller (8%). Table V shows the torque and speed response criteria of the PI and the FLC controllers.

TABLE V. RESULTS OF EVALUATION RESPONSIBILITY

Controller	PI	FLC
Torque responses		
Shape	Same as i_{sq} current response	Same as i_{sq} current response
Torque ripple	8%	3%
Speed responses		
Accelerated setting time	2.2 (s)	2.2 (s)
Over-adjustment	0%	0%

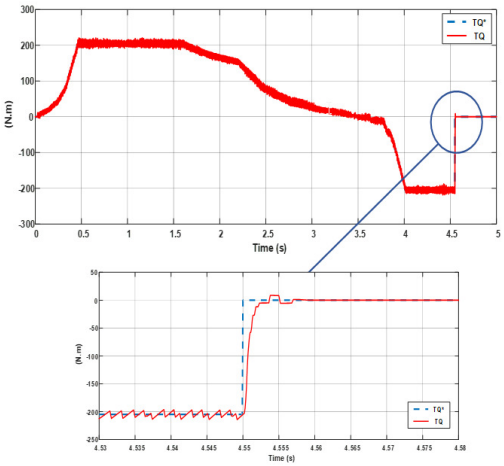

Fig. 8. Torque responses of the PI controller.

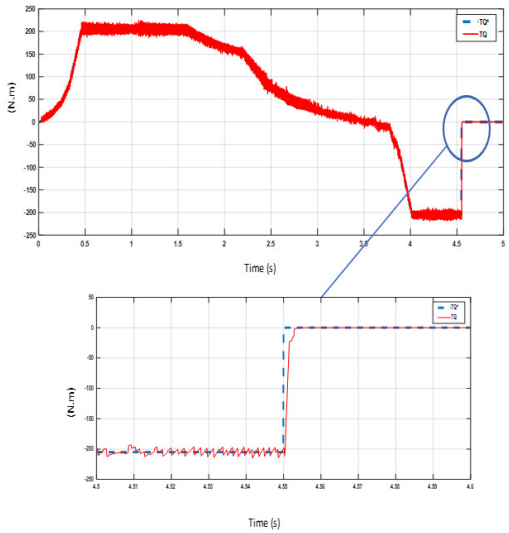

Fig. 9. Torque responses of the FCL controller.

Figure 10 shows the speed responses of an electric car transmission system using the PI controller and the FLC. The actual speed response of an electric car in both cases is in line

with the set requirements, and the speed response does not have too much speed adjustment at starting, accelerating, and decelerating.

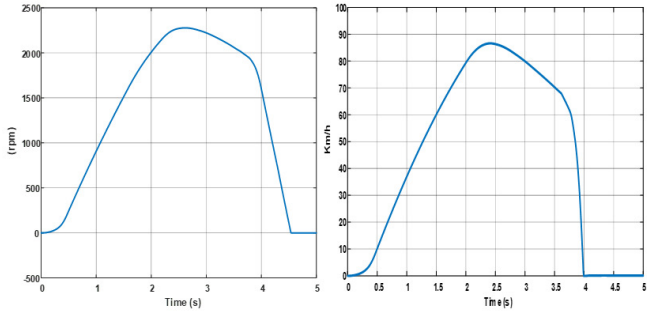

Fig. 10. Speed responses of the PI controller and the FLC.

V. CONCLUSION

This paper presented an in-wheel AFPMSM motor torque controller design for a traction drive system using a fuzzy logic control method. The proposed controller was compared with the PI controller and its efficiency was demonstrated through MATLAB simulations. The proposed controller provides better torque and speed response results than the PI controller in terms of steady-state time, over-adjustment, and torque pulsation. However, this controller has a complicated design, so it is necessary to study more simple but intelligent control solutions in the future.

ACKNOWLEDGMENT

This study was funded by the University of Transport and Communications (UTC) under grant number T2023-DT-001TD.

REFERENCES

[1] X. Zhang, D. Göhlich, and J. Li, "Energy-Efficient Toque Allocation Design of Traction and Regenerative Braking for Distributed Drive Electric Vehicles," *IEEE Transactions on Vehicular Technology*, vol. 67, no. 1, pp. 285–295, Jan. 2018, https://doi.org/10.1109/TVT.2017.2731525.

[2] N. Mutoh, "Driving and Braking Torque Distribution Methods for Front- and Rear-Wheel-Independent Drive-Type Electric Vehicles on Roads With Low Friction Coefficient," *IEEE Transactions on Industrial Electronics*, vol. 59, no. 10, pp. 3919–3933, Jul. 2012, https://doi.org/10.1109/TIE.2012.2186772.

[3] X. Yuan and J. Wang, "Torque Distribution Strategy for a Front- and Rear-Wheel-Driven Electric Vehicle," *IEEE Transactions on Vehicular Technology*, vol. 61, no. 8, pp. 3365–3374, Jul. 2012, https://doi.org/10.1109/TVT.2012.2213282.

[4] R. Wrobel, J. Goss, A. Mlot, and P. H. Mellor, "Design Considerations of a Brushless Open-Slot Radial-Flux PM Hub Motor," *IEEE Transactions on Industry Applications*, vol. 50, no. 3, pp. 1757–1767, Feb. 2014, https://doi.org/10.1109/TIA.2013.2284298.

[5] W. Xu, J. Zhu, Y. Guo, S. Wang, Y. Wang, and Z. Shi, "Survey on electrical machines in electrical vehicles," in *2009 International Conference on Applied Superconductivity and Electromagnetic Devices*, Chengdu, China, Sep. 2009, pp. 167–170, https://doi.org/10.1109/ASEMD.2009.5306667.

[6] M. A. Khlifi, M. B. Slimene, A. Alradedi, and S. A. Ahmadi, "Investigation of a Leakage Reactance Brushless DC Motor for DC Air Conditioning Compressor," *Engineering, Technology & Applied Science Research*, vol. 12, no. 2, pp. 8316–8320, Apr. 2022, https://doi.org/10.48084/etasr.4762.

[7] M. Yildirim, M. Polat, and H. Kürüm, "A survey on comparison of electric motor types and drives used for electric vehicles," in *2014 16th International Power Electronics and Motion Control Conference and Exposition*, Antalya, Turkey, Sep. 2014, pp. 218–223, https://doi.org/10.1109/EPEPEMC.2014.6980715.

[8] T. A. Zarma, A. A. Galadima, and M. A. Aminu, "Review of Motors for Electric Vehicles," *Journal of Scientific Research and Reports*, vol. 24, no. 6, pp. 1–6, Oct. 2019, https://doi.org/10.9734/jsrr/2019/v24i630170.

[9] X. del T. Garcia, B. Zigmund, A. A. Terlizzi, R. Pavlanin, and L. Salvatore, "Comparison between FOC and DTC Strategies for Permanent Magnet Synchronous Motors," *Advances in Electrical and Electronic Engineering*, vol. 5, no. 1, pp. 76–81, Jun. 2011.

[10] P. Bhatt, H. Mehar, and M. Sahajwani, "Electrical Motors for Electric Vehicle – A Comparative Study," in *Proceedings of Recent Advances in Interdisciplinary Trends in Engineering & Applications (RAITEA) 2019*, Apr. 2019, https://doi.org/10.2139/ssrn.3364887.

[11] M. Aydin and M. Gulec, "A New Coreless Axial Flux Interior Permanent Magnet Synchronous Motor With Sinusoidal Rotor Segments," *IEEE Transactions on Magnetics*, vol. 52, no. 7, pp. 1–4, Jul. 2016, https://doi.org/10.1109/TMAG.2016.2522950.

[12] W. Yu and C. Gu, "Dynamic analysis of a novel clutch system for in-wheel motor drive electric vehicles," *IET Electric Power Applications*, vol. 11, no. 1, pp. 90–98, 2017, https://doi.org/10.1049/iet-epa.2016.0270.

[13] A. Darba, M. Esmalifalak, and E. S. Barazandeh, "Implementing SVPWM technique to axial flux permanent magnet synchronous motor drive with internal model current controller," in *2010 4th International Power Engineering and Optimization Conference (PEOCO)*, Shah Alam, Malaysia, Jun. 2010, pp. 126–131, https://doi.org/10.1109/PEOCO.2010.5559197.

[14] R. Krishnan, *Electric Motor Drives: Modeling, Analysis, and Control*, 1st edition. Upper Saddle River, N.J: Pearson, 2001.

[15] P. T. Giang, V. T. Ha, and V. H. Phuong, "Drive Control of a Permanent Magnet Synchronous Motor Fed by a Multi-level Inverter for Electric Vehicle Application," *Engineering, Technology & Applied Science Research*, vol. 12, no. 3, pp. 8658–8666, Jun. 2022, https://doi.org/10.48084/etasr.4935.

[16] V. T. Ha, P. T. Giang, and V. H. Phuong, "T-Type Multi-Inverter Application for Traction Motor Control," *Engineering, Technology & Applied Science Research*, vol. 12, no. 2, pp. 8321–8327, Apr. 2022, https://doi.org/10.48084/etasr.4776.

[17] V. Q. Vinh and V. T. Ha, "Improved Torque Ripple of Switched Reluctance Motors using Sliding Mode Control for Electric Vehicles," *Engineering, Technology & Applied Science Research*, vol. 13, no. 1, pp. 10140–10144, Feb. 2023, https://doi.org/10.48084/etasr.5559.

[18] T. D. Nguyen, K.-J. Tseng, S. Zhang, and H. T. Nguyen, "A Novel Axial Flux Permanent-Magnet Machine for Flywheel Energy Storage System: Design and Analysis," *IEEE Transactions on Industrial Electronics*, vol. 58, no. 9, pp. 3784–3794, Sep. 2011, https://doi.org/10.1109/TIE.2010.2089939.

[19] T. D. Nguyen, G. F. H. Beng, K.-J. Tseng, D. M. Vilathgamuwa, and X. Zhang, "Modeling and Position-Sensorless Control of a Dual-Airgap Axial Flux Permanent Magnet Machine for Flywheel Energy Storage Systems," *Journal of Power Electronics*, vol. 12, no. 5, pp. 758–768, 2012, https://doi.org/10.6113/JPE.2012.12.5.758.

[20] Q. D. Nguyen and S. Ueno, "Analysis and Control of Nonsalient Permanent Magnet Axial Gap Self-Bearing Motor," *IEEE Transactions on Industrial Electronics*, vol. 58, no. 7, pp. 2644–2652, Jul. 2011, https://doi.org/10.1109/TIE.2010.2076309.